Magnetic linear response properties calculations with the Gaussian and augmented-plane-wave method

Valéry Weber,[1,a)] Marcella Iannuzzi,[1] Samuele Giani,[1] Jürg Hutter,[1] Reinout Declerck,[2] and Michel Waroquier[2]
[1]*Institute of Physical Chemistry, University of Zurich, Winterthurerstr. 190, CH-8057 Zurich, Switzerland*
[2]*Center for Molecular Modeling, Ghent University, Proeftuinstraat 86, B-9000 Gent, Belgium*

(Received 6 January 2009; accepted 1 June 2009; published online 7 July 2009)

We introduce a method for the all-electron calculation of the NMR chemical shifts and the EPR *g* tensor using the Gaussian and augmented-plane-wave method. The presented approach is based on the generalized density functional perturbation theory. The method is validated by comparison with other theoretical methods for a selection of small molecules. We also present two exemplary applications that involve the calculation of the chemical shifts of a hydrated adenine and the *g* tensor for the E_1' center in α-quartz using a quantum mechanical/molecular mechanical approach.
 [DOI: 10.1063/1.3156803]

I. INTRODUCTION

Nuclear magnetic resonance (NMR) and electron paramagnetic resonance (EPR) are two of the most powerful spectroscopic techniques, providing invaluable insights in the atomic structure of materials across a broad range of scientific disciplines. In recent years, there has been a growing interest in the *ab initio* quantum mechanical calculation of the quantities extracted from NMR/EPR spectra within the Kohn–Sham density functional theory (DFT).[1,2] A comprehensive overview of the various approaches in this field is given in Ref. 3. By comparing the experimental NMR/EPR quantities with those computed from proposed molecular models, it is possible to identify and understand the molecular structure. In particular, the possibility to derive structure/spectroscopic correlations from, e.g., molecular dynamics provides a basis for determining numerous aspects of the molecular structure and its related properties, such as chemical bonding and chemical reactions, which are not readily accessible from experiment.

However, many interesting scientific problems that would potentially benefit from a theoretical NMR/EPR study involve simulations that easily require many thousands of atoms, such as nanostructures, interfaces, molecular liquids, and complex biomolecules in their natural environment. Thus, there is still the need for developing efficient algorithms for the calculations of such properties for systems containing many thousands of atoms. Recently, Ochsenfeld *et al.*[4] and Kussmann and Ochsenfeld[5] introduced a method for the computation of chemical shifts for gas phase systems that scales linearly with the number of atoms. The authors report a large Hartree–Fock NMR calculation of N-methyl nicotinamide surrounded by water molecules with a total of 1003 atoms.

We introduce a method for the calculation of NMR chemical shifts and EPR *g* tensors based on the Gaussian and augmented-plane-wave (GAPW)[6–8] formalism in its all-electron (AE) version. A key step in the calculation of the aforementioned magnetic properties is the capability to compute the induced current density generated by the external static magnetic perturbation. The present approach relies on density function perturbation theory (DFPT).[9–12]

A previous implementation of the DFPT, in a plane wave framework, has been successfully applied to the calculation of the chemical shift[13–15] as well as to the *g* tensor[16] in condensed matter. However, since the original technique makes use of the plane wave plus pseudopotential representation of the electronic structure, its applications have been restricted to light elements.

The development of the DFPT within the GAPW formalism allows an all electron description of the induced current density, thus lifting the main drawback of the plane wave implementations.[13,17] To this purpose, it is necessary to extend the concepts of the GAPW representation of the electronic density to the current density induced by the external magnetic field. To our knowledge, the gauge-including projector augmented wave (GIPAW) method[18,19] is the only other AE method (using a frozen-core approach) currently able to calculate these quantities for condensed phase systems using periodic boundary conditions (PBCs).

The proposed method differs from the work by Sebastiani and Parrinello[13] and Mauri *et al.*[17] in a few respects. It represents the electronic structure with local atomic centered Gaussian functions allowing for reduced complexity algorithms. Thus large scale calculations of the NMR and EPR parameters become feasible. The all electron description of the system permits the evaluations of the chemical shifts and *g* tensor for all elements. The use of localized orbitals for the evaluation of the magnetic properties within PBC was originally introduced by Sebastiani and Parrinello.

Among all the different methods available in the literature (see, e.g., Ref. 3), the gauge-including atomic orbital (GIAO) introduced by London[20] and first adopted for quantum chemical calculation of the NMR parameters by Ditchfield[21] is known to be the best for evaluating NMR

a)Electronic mail: vweber@pci.uzh.ch.

shifts. Despite the superiority of the GIAO approach, we chose the individual gauge for atoms in molecules (IGAIM) approach introduced by Keith and Bader[22] and the continuous set of gauge transformation (CSGT) approach by the same authors.[23] This choice was driven by the simplicity of the implementation of the IGAIM and CSGT compared to the GIAO approach. We can also note that the implementation of the hyperfine coupling tensor has been recently presented within the GAPW formalism.[24]

The structure of this paper is as follows: First, the theoretical aspects of the method are elaborated, with particular attention on features that are specifically related to the GAPW representation. This includes the decomposition of the current density in soft and hard terms, the convergence with respect to basis set size, and the choice of the gauge. Then, the accuracy of the approach is presented by comparing the results obtained for a set of small isolated molecules to the values obtained from well-established methods commonly used for NMR and EPR calculations.

Finally, two exemplary applications are presented. The first application presents a quantum mechanical/molecular mechanical (QM/MM) calculations of the NMR shifts of an adenine molecule hydrated with 827 water molecules. In this example, the QM part contains up to 66 atoms. The second shows the calculation of the g tensor for the E_1' center in α-quartz using a 15 551-atom simulation cell and a three-layered AE DFT/pseudopotential DFT/molecular mechanics (AE/PSP/MM) approach. The QM (AE/PSP) part of this calculation contains 159 atoms.

II. THEORY

The xy-components of the chemical shift tensor σ^A corresponding to nucleus A and the g tensor for systems with net electronic spin 1/2, can be evaluated through the following expressions (note that atomic units will be adopted throughout this paper):

$$\sigma_{xy}^A = \frac{1}{c}\int_{\Omega_S}\left[\frac{\mathbf{r}-\mathbf{A}}{|\mathbf{r}-\mathbf{A}|^3}\times\mathbf{j}_x(\mathbf{r})\right]_y d^3r \tag{1}$$

and

$$g_{xy} = g_{xy}^{\mathrm{Z}} + \Delta g_{xy}^{\mathrm{ZKE}} + \Delta g_{xy}^{\mathrm{SO}} + \Delta g_{xy}^{\mathrm{SOO}}, \tag{2}$$

where c is the speed of light in vacuum, $\mathbf{A}$ is the position of the nucleus A, $\mathbf{j}_x$ is the current density induced by a constant external magnetic field applied along the x axis, and Ω_S is the volume of the whole integration domain, including the periodic replicas of the simulation cell. The other tensor components can be obtained by changing the indices accordingly. The different contributions to the g tensor are

$$g_{xy}^{\mathrm{Z}} = g_e\delta_{xy}, \tag{3}$$

$$\Delta g_{xy}^{\mathrm{ZKE}} = -\frac{g_e}{c^2}(T^\alpha - T^\beta)\delta_{xy}, \tag{4}$$

$$\Delta g_{xy}^{\mathrm{SO}} = \frac{(g_e-1)}{c}\int_{\Omega_C}[\mathbf{j}_x^\alpha(\mathbf{r})\times\nabla V_{\mathrm{eff}}^\alpha(\mathbf{r}) - \mathbf{j}_x^\beta(\mathbf{r}) \times\nabla V_{\mathrm{eff}}^\beta(\mathbf{r})]_y d^3r, \tag{5}$$

and

$$\Delta g_{xy}^{\mathrm{SOO}} = 2\int_{\Omega_C} B_{xy}^{\mathrm{corr}}(\mathbf{r})\rho^s(\mathbf{r})d^3r, \tag{6}$$

where g_e denotes the free-electron g value, $\rho^s=\rho^\alpha-\rho^\beta$ is the spin density, α and β denoting the spin channels, and T^α, $\mathbf{j}_x^\alpha$, and ρ^α are the unperturbed kinetic energy, induced current density, and electron density of the spin-α channel, respectively. In this case the integrals span only the volume of the simulation cell, Ω_C. V_{eff}^α is an effective potential in which the spin-α electrons are thought to move (see the Appendix for more details). $\mathbf{B}_x^{\mathrm{corr}}$ represents the magnetic field that originates from the corresponding total induced current density $\mathbf{j}_x$ and is given by

$$\mathbf{B}_x^{\mathrm{corr}}(\mathbf{r}) = \frac{1}{c}\int_{\Omega_S}\frac{\mathbf{r}'-\mathbf{r}}{|\mathbf{r}'-\mathbf{r}|^3}\times(\mathbf{j}_x(\mathbf{r}') - \mathbf{j}_x^s(\mathbf{r}'))d^3r', \tag{7}$$

where the subtraction of $\mathbf{j}_x^s=\mathbf{j}_x^\alpha-\mathbf{j}_x^\beta$ is introduced as a self-interaction correction.

It is readily apparent from Eqs. (1)–(7) that the induced current densities are a key ingredient in the evaluation of NMR and EPR properties. In the following subsections, after a brief recapitulation of the essential ideas of the GAPW representation, we describe first how the induced current densities can be derived in DFPT as applied within the GAPW formalism and then we turn our attention to the actual evaluation of the tensor components.

A. The GAPW representation of the electron density

In the GAPW density functional method,[6–8] the electron density ρ is defined by its expansion in atomic orbitals χ_k,

$$\rho(\mathbf{r}) = \sum_{kl} P_{kl}\chi_k(\mathbf{r})\chi_l(\mathbf{r}),$$

where k and l run over the basis functions and the element of the density matrix is defined as $P_{kl}=\Sigma_i C_{ki}^{(0)}C_{li}^{(0)}$. The elements of $C^{(0)}$ are the expansion coefficients of the unperturbed (ground state) orbitals $\psi^{(0)}$. As atomic orbitals we employ contracted Gaussian functions, i.e., a linear combination of atom-centered primitive Cartesian Gaussian functions.

The simulation cell is now divided into nonoverlapping, localized, spherical regions centered on the atomic nuclei and an interstitial region. The underlying idea in GAPW is that the electron density varies smoothly in the interstitial region and is therefore easily representable in a plane wave basis, whereas the quickly varying electron density near the nuclei is more efficiently manipulated in terms of localized functions. Following the projector augmented-wave approach introduced by Blöchl,[25] the GAPW representation of the electron density can be written as a sum of three contributions,

$$\rho(\mathbf{r}) = \tilde{\rho}(\mathbf{r}) + \sum_A (\rho_A(\mathbf{r}) - \tilde{\rho}_A(\mathbf{r})),$$

where $\tilde{\rho}$ is a soft density and ρ_A and $\tilde{\rho}_A$ are local atom-centered hard and soft densities, respectively. All densities are defined over the entire space. The resulting double counting is compensated by constructing the soft local atomic densities $\tilde{\rho}_A$ such that their sum $\Sigma_A \tilde{\rho}_A$ equals the soft density $\tilde{\rho}$ within the atomic spherical regions, while in the interstitial region it is equivalent to $\Sigma_A \rho_A$.

B. Calculation of the induced current densities

The linear response of the electronic structure due to the application of an external magnetic field can be determined by solving a system of linear equations of the type

$$-\mathrm{i}\sum_{il}\left(H_{kl}\delta_{ij} - S_{kl}\int \psi_i^{(0)}(\mathbf{r})H(\mathbf{r})\psi_j^{(0)}(\mathbf{r})d^3r\right)C_{li}^{(1)} = \sum_l H_{kl(j)}^{(1)}C_{lj}^{(0)},$$

where the index i runs over the occupied ground state orbitals, H_{kl} is a matrix element of the unperturbed Hamiltonian, S_{kl} is an element of the overlap matrix, $H_{kl}^{(1)}$ is a matrix element of the perturbation operator, and the matrix $C^{(1)}$ is the matrix of the expansion coefficients of the corresponding linear response of the orbitals, $\psi^{(1)}$. Note that the imaginary nature of the response orbital has been made explicit, allowing us to work with real expansion coefficients also for the response orbitals. The optional subindex (j), labeling the matrix element of the perturbation operator, indicates that the perturbation might be orbital dependent. In the case of interest here, the perturbation can be split into three different types of operators, which are $(\mathbf{r}-\mathbf{d}_j)\times\mathbf{p}$, the *orbital angular momentum* operator (which leads to the response orbitals C^L), $\mathbf{p}$ the *momentum* operator (leading to C^p), and $(\mathbf{d}_i-\mathbf{d}_j)\times\mathbf{p}$ the *full correction* operator (leading to $C^{\Delta i}$). In the notation, the vector $\mathbf{d}_j$ is the Wannier center associated with the unperturbed jth orbital. It makes the angular momentum and the full correction perturbation operators dependent on the unperturbed orbital to which they are applied. In conclusion, the linear response orbitals are then given by nine sets of expansion coefficients, C^L, C^p, and $C^{\Delta i}$, as for each operator the three Cartesian components are considered. The matrix elements of the perturbation operator are

$$H_{klj}^L = -\mathrm{i}\int \chi_k(\mathbf{r})(\mathbf{r}-\mathbf{d}_j)\times\nabla\chi_l(\mathbf{r})d^3r,$$

$$H_{kl}^p = -\mathrm{i}\int \chi_k(\mathbf{r})\,\nabla\,\chi_l(\mathbf{r})d^3r,$$

and

$$H_{klj}^{\Delta i} = -\mathrm{i}(\mathbf{d}_i-\mathbf{d}_j)\times\int \chi_k(\mathbf{r})\,\nabla\,\chi_l(\mathbf{r})d^3r.$$

We can note here that for a magnetic field as a perturbation, the first order change in the charge density vanishes everywhere in space. Thus, this perturbation does not give rise to a first order change in the Hartree and exchange-correlation terms. This simplifies considerably the linear system of equations and is often called uncoupled perturbed self-consistent field equations.

Once all the contributions to the linear response orbitals have been calculated, the x-component of the linear current density response induced from an external magnetic field applied along the y axis can be written as

$$j_{xy}(\mathbf{r}) = -\frac{1}{2c}\sum_{ikl}[C_{ki}^{(0)}(C_{li}^{L_y} + (d(\mathbf{r})-\mathbf{d}_i)_x C_{li}^{p_z} - (d(\mathbf{r})-\mathbf{d}_i)_z C_{li}^{p_x} - C_{li}^{\Delta i_y}) \times\{(\nabla_x\chi_k(\mathbf{r}))\chi_l(\mathbf{r}) - \chi_k(\mathbf{r})\nabla_x\chi_l(\mathbf{r})\}] + (\mathbf{r}-d(\mathbf{r}))_z\rho(\mathbf{r}), \quad (8)$$

where $d(\mathbf{r})$ is a gauge that will be discussed in the following sections of this work. While the first term (square brackets) on the right-hand side of Eq. (8) represents the paramagnetic contribution to the current density, the second term is the diamagnetic part. The latter vanishes identically when the CSGT approach[23] is employed, i.e., $d(\mathbf{r})=\mathbf{r}$. The other components of the current density are obtained in an analogous way by changing appropriately the Cartesian indices.

1. The position operator in PBC

The position operator $\mathbf{r}$ operating on a (one-particle) wave function in the coordinate representation $\psi(\mathbf{r})$ results in the multiplication of this wave function with the position variable $\mathbf{r}$. When PBCs are imposed, the multiplicative position operator is not a valid operator, since the Cartesian components of $\mathbf{r}\psi(\mathbf{r})$ are no longer periodic.[26] In the derivation of the response orbitals, the position operator appears in the definition of the perturbation operators and in the definition of the current density. To solve this problem, we maximally localize the ground state orbitals.[27–29] For insulators, these Wannier functions feature an exponential decay[30] and can be considered as confined for sufficiently large simulation cells. As described in Ref. 13, the position operator can be redefined to obey the PBC by using a sawtooth-shaped profile centered at the Wannier center of the localized orbital to which it is applied, thus taking advantage of the translational freedom in setting the origin of the coordinate system.

2. GAPW representation of the induced current densities and gauge

In the GAPW framework, we propose to use for the induced current density a decomposition analogous to the one applied to the electron density,

$$\mathbf{j}(\mathbf{r}) = \tilde{\mathbf{j}}(\mathbf{r}) + \sum_A (\mathbf{j}_A(\mathbf{r}) - \tilde{\mathbf{j}}_A(\mathbf{r})),$$

where $\tilde{\mathbf{j}}$ is the soft contribution to the total current density, $\mathbf{j}_A$ is the local hard contribution centered on atom A, and $\tilde{\mathbf{j}}_A$ is the local soft contribution, which compensates for the double counting.

The convergence of the NMR chemical shifts with respect to Gaussian basis set size is strongly dependent on the

choice of the gauge $d(\mathbf{r})$, see e.g., Ref. 3 and references therein. It is thus important to judiciously choose the gauge that provides a good compromise between complexity and convergence with respect to the basis set size.

The advantage of the $d(\mathbf{r})=\mathbf{r}$ gauge (CSGT), i.e., that the diamagnetic term is identically zero, can be significantly weakened due to the rich basis set required to obtain an accurate description of the current density close to the nuclei. Thus, it seemed more appropriate to implement the IGAIM approach[22] following the procedure by Cheeseman *et al.*[31] In the IGAIM method, the gauge $d(\mathbf{r})$ is taken as the closest nuclear center.

It is interesting to notice that, in contrast with the chemical shift calculations, the evaluation of the g tensor is less affected by the choice of the gauge even when the simpler and computationally more convenient CSGT approach is used.

C. Calculation of the chemical shift tensor

The computation of the chemical shift tensor requires the evaluation of the integral Eq. (1). This can efficiently be done using the GAPW representation of the induced current density response.

The contribution to the chemical shift coming from the soft part of the induced current density response $\tilde{\mathbf{j}}$ is computed in reciprocal space. Following the procedure suggested by Pickard and Mauri[18] and Sebastiani and Parrinello,[13] we distinguish between the $\mathbf{G}\neq\mathbf{0}$ components and the $\mathbf{G}=\mathbf{0}$ component of the induced magnetic field, where $\mathbf{G}$ denotes a reciprocal space vector. It is observed that the $\mathbf{G}=\mathbf{0}$ component, which cannot be computed within PBC, depends on the macroscopic shape of the studied material. By assuming a spherical shape, it can be approximated, computing the magnetic susceptibility arising from the soft induced current density $\tilde{\mathbf{j}}$, as

$$\chi_{xy}=\frac{2\pi}{\Omega_c c}\int[\mathbf{r}\times\tilde{\mathbf{j}}_x(\mathbf{r})]_y d^3r. \tag{9}$$

The contribution to the chemical shift of the Ath nucleus, σ_{xy}^A, arising from the induced local current densities is evaluated as

$$\frac{1}{c}\sum_B\int_{\Omega_B}\left[\frac{\mathbf{r}-\mathbf{A}}{|\mathbf{r}-\mathbf{A}|^3}\times(\mathbf{j}_{xB}(\mathbf{r})-\tilde{\mathbf{j}}_{xB}(\mathbf{r}))\right]_y d^3r, \tag{10}$$

where the sum over B is restricted to the nuclei that are within a radius R_c from A. A discussion of the truncation of the summation will be given below. The integration over Ω_B is performed numerically on a spherical grid featuring a logarithmic radial and a Lebedev-type[32,33] angular discretization. The numerical integration converges rapidly with respect to the number of grid points and about 10 000 grid points per atom are enough to converge the chemical shifts below 10^{-1} ppm.

D. Calculation of the *g* tensor

The spin-orbit term (5), $\Delta g_{xy}^{\mathrm{SO}}$, is obtained essentially from integrating products of the induced current densities and the gradient of the effective potential V_{eff}^{τ} over the simulation cell. The calculation of the current density for each separate spin channel follows the procedure elaborated in Sec. II B. The effective potential V_{eff}^{τ} $(\tau=\alpha,\beta)$ (Ref. 34) is defined as

$$V_{\mathrm{eff}}^{\tau}(\mathbf{r})=v_{\mathrm{ext}}(\mathbf{r})+v_{\mathrm{H}}(\mathbf{r})+v_{xc}^{\tau}(\mathbf{r}),$$

where v_{ext} denotes the Coulombic potential from the nuclei, v_{H} the Hartree potential, and v_{xc}^{τ} the exchange-correlation potential. For further elaboration the Dirac/Slater exchange potential $v_{X_\alpha}^{\tau}$ (Ref. 35) is used. The use of $v_{X_\alpha}^{\tau}$ has been suggested by Schreckenbach and Ziegler[34] because of the lack of code for the required generalized gradient approximation (GGA) contributions. In principle, the extension with GGA functionals is feasible. However, it would require additional implementation efforts as the analytical gradients for each function should first be derived and then programmed for evaluation onto the different numerical grids (i.e., atomic-centered and FFT). Notwithstanding the scientific interest to assess the influence of choosing different exchange-correlation functionals, we have not given it the highest priority.

Using the technique elaborated in Ref. 25, the effective potential V_{eff}^{τ} is split into independent global and local atom-centered components. Appropriate screening densities[25] are used to construct the local components such that they remain limited to a small region around the atomic nuclei.

The working equation for the evaluation of $\Delta g_{xy}^{\mathrm{SO}}$ is

$$\begin{aligned}\Delta g_{xy}^{\mathrm{SO}}=\frac{g'}{2c}\Bigg\{&\int[\tilde{\mathbf{j}}_x^{\alpha}(\mathbf{r})\times\nabla\tilde{V}_{\mathrm{eff}}^{\alpha}(\mathbf{r})-\tilde{\mathbf{j}}_x^{\beta}(\mathbf{r})\times\nabla\tilde{V}_{\mathrm{eff}}^{\beta}(\mathbf{r})]_y d^3r\\&+\sum_A\int_{U_A}[(\mathbf{j}_{xA}^{\alpha}(\mathbf{r})-\tilde{\mathbf{j}}_{xA}^{\alpha}(\mathbf{r}))\times\nabla\tilde{V}_{\mathrm{eff}}^{\alpha}(\mathbf{r})\\&-(\mathbf{j}_{xA}^{\beta}(\mathbf{r})-\tilde{\mathbf{j}}_{xA}^{\beta}(\mathbf{r}))\times\nabla\tilde{V}_{\mathrm{eff}}^{\beta}(\mathbf{r})]_y d^3r\\&+\sum_A\int_{U_A}[\mathbf{j}_{xA}^{\alpha}(\mathbf{r})\times\nabla V_{\mathrm{eff}A}^{\alpha}(\mathbf{r})-\mathbf{j}_{xA}^{\beta}(\mathbf{r})\times\nabla V_{\mathrm{eff}A}^{\beta}(\mathbf{r})]_y d^3r\Bigg\},\end{aligned}$$

where the definition of the terms derived from the effective potential are similar to the one introduced in Ref. 25 (see also the Appendix for more details). The second integral of the above equation contains the soft components $\nabla\tilde{V}_{\mathrm{eff}}^{\tau}$. These are only available on the FFT grid, but need to be multiplied with the spin-current densities defined on the atom-centered grids of each atomic nucleus A. This problem is circumvented through a linear interpolation of the values of $\nabla\tilde{V}_{\mathrm{eff}}^{\tau}$ from the FFT-grid to the atom-centered grid.

The computation of the induced magnetic field $\mathbf{B}_x^{\mathrm{corr}}$ Eq. (7), required for the evaluation of the spin-other-orbits term $\Delta g_{xy}^{\mathrm{SOO}}$ Eq. (6), employs many of the techniques already used in the calculation of the chemical shift tensor. For the chemical shift tensor, only the positions of the atomic nuclei are of interest, whereas here the induced magnetic field must be known in the entire space. Unfortunately, due to the presence of a nonlocal operator, i.e., $\mathbf{r}'-\mathbf{r}/|\mathbf{r}'-\mathbf{r}|^3$, the creation of a GAPW representation for the induced magnetic field is not straightforward. In addition, the analytic elaboration through

the Gaussian representation of the current density is also far from trivial. However, it generally holds that $\Delta g_{xy}^{\mathrm{SOO}}$ is a relatively small term in comparison with $\Delta g_{xy}^{\mathrm{ZKE}}$ and $\Delta g_{xy}^{\mathrm{SO}}$.[19] For this reason, we choose to neglect the contributions from the atom-centered current densities $\mathbf{j}_{xA}^{\mathrm{corr}} - \tilde{\mathbf{j}}_{xA}^{\mathrm{corr}}$ to the $\mathbf{G} \neq \mathbf{0}$ components $\tilde{\mathbf{B}}_{x,\mathbf{G}\neq\mathbf{0}}^{\mathrm{corr}}$ of the induced magnetic field. Being computed from the soft current density $\tilde{\mathbf{j}}_{x}^{\mathrm{corr}}$ only, on the reciprocal-space FFT-grid, these components will be soft too (hence the tilde). $\mathbf{B}_{x,\mathbf{G}=\mathbf{0}}^{\mathrm{corr}}$, on the other hand, will be computed analytically via Eq. (9), using the Gaussian representation of the current density. In summary, $\Delta g_{xy}^{\mathrm{SOO}}$ is evaluated as follows:

$$\Delta g_{xy}^{\mathrm{SOO}} \approx 2\int_{\mathrm{FFT}} \tilde{B}_{xy,\mathbf{G}\neq\mathbf{0}}^{\mathrm{corr}}(\mathbf{r})\tilde{\rho}_{\mathrm{s}}(\mathbf{r})d^3r + 2\sum_A \int_{U_A} \tilde{B}_{xy,\mathbf{G}\neq\mathbf{0}}^{\mathrm{corr}}(\mathbf{r}) \times(\rho_A^{\mathrm{s}}(\mathbf{r}) - \tilde{\rho}_A^{\mathrm{s}}(\mathbf{r}))d^3r + 2B_{xy,\mathbf{G}=\mathbf{0}}^{\mathrm{corr}}.$$

III. RESULTS AND DISCUSSION

A. Test calculations

All developments were implemented in QUICKSTEP, which is part of CP2K.[36] CP2K is a freely available under the GNU General Public License (GPL) general program to perform atomistic and molecular simulations of solid state, liquid, molecular, and biological systems. A description of QUICKSTEP can be found in Ref. 37.

The GAPW method for the AE calculation of the NMR chemical shifts and the EPR g tensor was validated by comparison, for a series of small isolated molecules, with the results from conceptually similar gas-phase methods, (i) the NMR routines as implemented in the G03 program package[38] (further referred to as the IGAIM-GA method), and (ii) the g tensor method of Schreckenbach and Ziegler[34] as implemented in the ADF (Ref. 39) program package (further referred to as the SZ method). Isolated molecules are approximated by a supercell approach with a large cell size of $(20\ \text{Å})^3$. We used a 300 Ry cutoff for the auxiliary plane wave grid, the BLYP[40,41] gradient-corrected exchange-correlation functional, and the efficient and numerically stable orbital transformation energy minimizer introduced in Ref. 42. The Gaussian basis sets used in this work were taken from the Environmental Molecular Sciences Laboratory (EMSL) basis set exchange library.[43]

1. NMR

A comparison between the IGAIM method implemented in G03 (IGAIM-GA) and the presented IGAIM-GAPW method for the isotropic and the anisotropic chemical shifts of a representative set of small molecules is shown in Fig. 1. Three different basis sets were used, namely, the Pople split-valence double-zeta plus polarization 6-31G(d,p),[44,45] and the augmented double and triple-zeta correlation consistent basis sets aug-cc-pVDZ and aug-cc-pVTZ, respectively[46–49]. The test set is composed of 26 molecules, namely: C_2H_2, CH_2O, CH_3Cl, CH_3F, CH_4, Cl_2, CO_2, F_2, FCl, H_2O_2, H_2O, H_2, H_2S, HCl, HCN, HCOOH, HF, HNO_3, N_2O, N_2, NH_3, NO_2, O_2, O_3, PH_3, and SO_2. All the geometries were optimized at the BLYP/aug-cc-pVDZ level of theory.

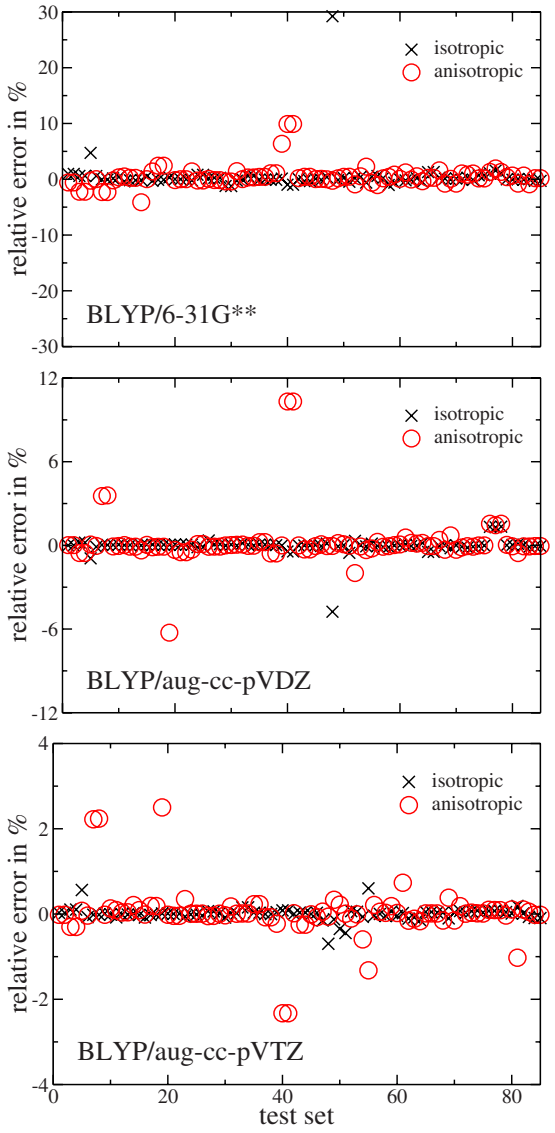

FIG. 1. Relative error of the IGAIM-GAPW method with respect to the IGAIM-GA method for the isotropic and anisotropic chemical shifts calculated on a set of small molecules (see text for details). Note the different scales in the three panels.

For the small 6-31G(d,p) basis set, a maximal unsigned relative error of 30% is observed for the isotropic chemical shift of the carbon atom in HCN. The isotropic shift for the nitrogen atom in HCN is 3.9 ppm for IGAIM-GA and 5.1 ppm for IGAIM-GAPW. This absolute error (1.2 ppm) is of the same order as for other nitrogen atoms with, e.g., 0.6 ppm for NH_3. Except for this extreme case, the other isotropic (anisotropic) chemical shifts have a smaller maximal unsigned relative error with, e.g., less than 1% (10%) for hydrogen, 5% (0.5%) for carbon, and 2% (2%) for oxygen.

The unsigned relative error is greatly reduced for the larger aug-cc-pVDZ and aug-cc-pVTZ basis sets. The aug-cc-pVDZ provides a maximal unsigned relative error of 5% (nitrogen in HCN) and 10% (H_2) for, respectively, the isotropic and anisotropic components of the shift. The maximal unsigned relative errors for the isotropic shift are 0.5%

TABLE I. Convergence of the isotropic chemical shifts of the central water molecule of a water chain (see text for details) with respect to the truncation parameter R_c introduced in Eq. (10). The H_1 atoms is aligned along the z-axis. All the values are in ppm.

	R_c=0.5 Å	R_c=1.6 Å	R_c=4.0 Å	All atoms
O	322.2247	322.2465	322.2489	322.2481
H_1	29.8431	29.5129	29.5829	29.5926
H_2	32.8875	32.1919	32.1276	32.1141

for hydrogen, 0.9% for carbon, 4.8% for nitrogen, 1.3% for oxygen, smaller than 0.1% for fluorine, silicon, and phosphorus, 0.1% for sulfur, and 0.2% for chlorine. The maximal unsigned relative error for the aug-cc-pVTZ basis set is 0.7% and 2.5% for the iso- and anisotropic part of the shift, respectively. For the different atomic kinds, we obtained a maximal unsigned relative error of 0.6% (H), 0.6% (C), 0.7% (N), 0.4% (O), and finally less than 0.1% (F, P, S, and Cl). The corresponding maximal absolute errors are 0.2 (H), 0.1 (C), 0.3 (N), 0.6 (O), 0.3 (F), 0.3 (P), 0.2 (S), and 0.1 ppm (Cl).

The relative accuracy of the chemical shifts mirrors the previous observations for the total energy.[8] This inaccuracy can be traced back to the incompleteness of the basis used to represent the local contribution of the atomic densities and the induced current densities. In the present implementation, this local basis is constructed from the primitive functions of the original basis set[6,7] and shows better convergence with increasing the quality of the basis set. Accordingly, the inaccuracy of the chemical shifts can be systematically reduced by increasing the quality of the basis employed to represent the local contributions.

For a given basis set, the inaccuracy depends on different factors such as the hybridization of the atom of interest and its chemical environment. Therefore, the accuracy of relative shifts might not be significantly improved.

In Table I, we present the convergence of the isotropic chemical shifts for a test case: The central molecule of a linear water chain with respect to the truncation parameter R_c introduced in Eq. (10). The calculations were carried out at the BLYP/aug-cc-pVTZ level of theory. This test system is composed of a linear chain consisting of nine hydrogen-bonded water molecules (both intramolecular O–H bond lengths of 0.95 Å and H–O–H angle of 109.47°) with an O–O distance of 3 Å. The $O-H_1$ bonds are aligned along the z-axis. Different radial cutoffs are chosen, increasing in size, to include in the summation [Eq. (10)], first the single atom where the shift is measured, then the central water molecule, the central and its first neighboring water molecules, and finally the full system. While the chemical shifts of the oxygen are not too sensitive to the truncation, the shifts of the proton are affected by small values of R_c with a worst case difference of up to 0.8 ppm for H_2. A truncation of R_c=4 Å gives error in the chemical shifts for the proton by less than 0.02 ppm. Except this test case, no truncation is used in the rest of this work.

2. EPR

For the g tensor, a true side-by-side comparison is not feasible, since ADF employs Slater-type basis functions.

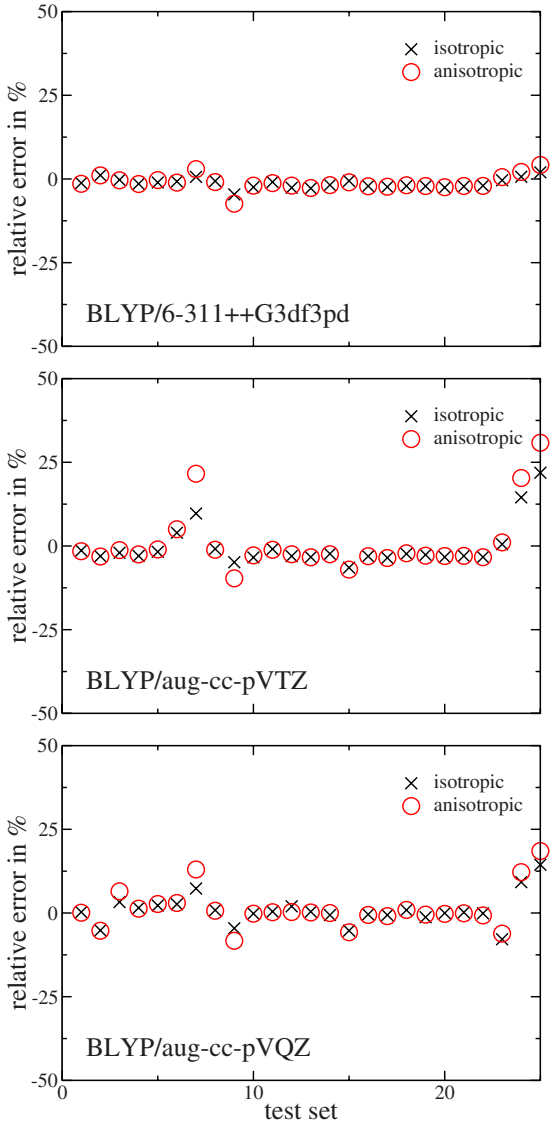

FIG. 2. Relative error of the CSGT-GAPW method with respect to the SZ method for the isotropic and anisotropic Δg values calculated on a set of small isolated molecules (see text for details).

Nevertheless, we calculated the g tensors with a very large et-pVQZ basis set to regard this as a fully converged set. The test set is composed of 25 isolated molecules, which are BO, BS, C_3H_5, CH_3, CH_4^+, ClO_2, ClO_3, CN, CO_2^-, CO_3^-, CO^+, H_2CO^+, H_2O^+, COH, MgF, NF_2, NF_3^+, NH_3^+, NO_2, NO_3, HO_2 (hydroperoxyl radical), O_3^-, SiH_3, SO_2^-, and SO_3^-. In Fig. 2, we compare with this reference set three different Gaussian basis sets, i.e., 6-311++G($3df$,$3pd$), aug-cc-pVTZ, and aug-cc-pVQZ. The $d(\mathbf{r})=\mathbf{r}$ gauge was employed for all the EPR calculations (referred as to CSGT-GAPW). The same geometry (optimized using ADF/et-pVQZ) was used throughout. A comparison between the SZ method and the CSGT-GAPW method for the isotropic and the anisotropic Δg values ($\Delta g=g-g_e$) of a comprehensive set of molecules is shown in Fig. 2. Just as it was the case for the chemical shifts, the Δg values are expressed in ppm. Using the 6-311++G($3df$,$3pd$) basis set, most Δg values agree to within a few percent, an excellent result, considered the very different basis sets used. For both the aug-cc-pVTZ and the

TABLE II. Percentage deviation of the CSGT-GAPW method from the SZ/et-pVQZ method for the isotropic and anisotropic Δg values of SO_3^- using different aug-cc-pVXZ basis sets.

	aug-cc-pVDZ	aug-cc-pVTZ	aug-cc-pVQZ	aug-cc-pV5Z
iso	38	22	14	8
ani	53	31	18	8

aug-cc-pVQZ basis set, most of the Δg values still agree to within better than 10% with the SZ results, but larger deviations (up to around 30% for the aug-cc-pVTZ basis sets) are obtained for ClO_3, SO_2^-, and SO_3^-. As shown in Table II, these errors seem to originate from a slower basis set convergence for the g tensor in the aug-cc-pVXZ series; only with an even larger aug-cc-pV5Z (Ref. 49) basis set for sulfur, a more satisfying agreement is obtained.

Finally, for a few selected small molecules, we also compare (Table III) with the GIPAW g-tensor method, as implemented in the QUANTUM-ESPRESSO program package,[50] using dedicated Troullier–Martins[51] pseudopotentials, a 100 Ry plane wave cutoff, PBE (Ref. 52) functional, and a similar supercell approach. Since the PBE-GIPAW pseudopotentials were readily available, the PBE functional was chosen for all the three methods. The results for the three selected molecules show very good agreement between the different methods.

B. Chemical shifts of isolated and hydrated adenine

To further validate the method, we present, in Table IV, the calculated chemical shifts for an isolated adenine. While the ^{15}N chemical shifts are referenced to $MeNO_2$, the ^1H and ^{13}C are given with respect to tetramethylsilane (TMS). The absolute chemical shifts for all the references are also reported in Table IV. The geometries of adenine and all the references were optimized at the BLYP/6-31G(d,p) level of theory. For the labeling scheme of adenine see Fig. 3.

For comparison, we also report a calculation with the method by Sebastiani and Parrinello (referred to as CSGT-CP) as implemented in CPMD.[53] In the calculations the BLYP functional, a plane wave cutoff of 200 Ry, and pseudopotential of the Goedecker type[54] were used. Chemical shifts corrected for the core electrons are also presented in parentheses. The core contribution to the pseudopotential calculations is assumed to be constant for an atom in a chemically "equivalent" environment. These corrections are calculated as[18]

$$\delta(X) = \sigma(X_{\text{ref}}) - \sigma(X) + \delta(X_{\text{ref}}),$$

where X is the atom considered, X_{ref} is the *same* atom in a reference system, the $\sigma(X_{\text{ref}})$ and $\sigma(X)$ are computed at the same level of theory, and $\delta(X_{\text{ref}})$ is the chemical shift of the reference system with respect to the external reference (here TMS or $MeNO_2$). In this work the $\delta(X_{\text{ref}})$ were calculated at the BLYP/aug-cc-pV5Z level of theory with the IGAIM-GA method. The reference systems are chosen to be benzene for all the carbon atoms, pyridine for N_1, N_3, and N_7, aniline for N_6, and pyrrole for N_9.

TABLE III. Comparison of the principal Δg values of three small isolated molecules obtained with the SZ, GIPAW, and the CSGT-GAPW methods. The PBE functional is used for all the three methods. All the values are in ppm.

		SZ	GIPAW	CSGT-GAPW
		et-pVQZ	TM/100 Ry	aug-cc-pVQZ
CH_4^+	$\Delta g_\parallel$	−55	−65	−60
	$\Delta g_\perp$	1058	924	1087
HO_2	Δg_{xx}	−290	−290	−258
	Δg_{yy}	6329	6110	6357
	Δg_{zz}	30 240	27 420	30 298
SiH_3	$\Delta g_\parallel$	−72	−108	−97
	$\Delta g_\perp$	2617	2261	2477

The IGAIM-GA and the IGAIM-GAPW calculations with the cc-pVQZ basis set give similar chemical shifts as expected from the benchmark shown above. While the ^{15}N and ^{13}C chemical shifts calculated with the CSGT-CP method can be in disagreement by up to 40 ppm with respect to the IGAIM-GA/aug-cc-pV5Z calculation, the corrected shifts are in much better agreement (except for N_1 with a difference of about 17 ppm) with the Gaussian based methods. For the ^1H chemical shifts, a large difference (up to 1 ppm) is observed between the Gaussian based and the CSGT-CP methods.

In the last column of Table IV, we also present the chemical shifts obtained with the GIPAW method, as implemented in the QUANTUM-ESPRESSO program package.[50] The PBE functional, the Troullier–Martins[51] GIPAW pseudopotentials, a $3\times3\times3$ k-point mesh, and a 100 Ry plane wave cutoff were used for the calculations. For the sake of comparison, we also show the chemical shifts obtained with the IGAIM-GAPW method at the PBE/cc-pVQZ level of theory. The shifts obtained with the IGAIM and GIPAW methods are in very good agreement. A deviation of 6 and 12 ppm can be seen for the carbon and nitrogen atoms, respectively. This disagreement is attributed to the quality of the basis set used for the IGAIM-GAPW calculation. The deviation for the chemical shift of the H_8 is surprisingly large (0.5 ppm).

To show further the capability of the implementation of the IGAIM-GAPW method, we present in Table V the chemical shifts of hydrated adenine calculated within the QM/MM framework and PBC. The full system contains the adenine and 827 water molecules. The coordinates of the system were extracted from a classical molecular dynamics simulation (see Ref. 55 for more details about the setup). The absolute chemical shifts of the reference systems, TMS, and $MeNO_2$ were taken from Table IV.

The first calculation, reported in the table, consists of the adenine without the solvent (further referred to as ISO) at the BLYP/cc-pVQZ level of theory. The next columns are obtained within the QM/MM framework with different QM regions, i.e., the adenine only (W0) and the adenine plus the water molecules overlapping spheres of 3 Å radius (W3) around each solute atoms and the same setup but with a radius of 5 Å (W5). We note that the ^{13}C chemical shifts are mostly insensitive to the presence of the solvent with a maxi-

TABLE IV. Calculated ^{13}C, ^{1}H, and ^{15}N chemical shifts of an isolated adenine (upper part of the table). Values in parentheses are corrected for core electrons (see text for details). Absolute chemical shifts of the references are shown in the lower part of the table. The subscripts *t*, *n*, *b*, *py*, *pr*, and *a* refer to TMS, $MeNO_2$, benzene, pyridine, pyrrole, and aniline, respectively. All the values are in ppm.

	IGAIM-GAPW[a]	IGAIM-GA[a]	IGAIM-GA[b]	CSGT-CP[c]	IGAIM-GAPW[d]	GIPAW[e]
C_2	164	164	166	136 (168)	162	166
C_4	159	159	162	130 (161)	156	162
C_5	128	128	130	93 (124)	126	131
C_6	163	163	165	134 (166)	161	164
C_8	141	141	143	115 (146)	140	143
H_2	8.4	8.4	8.5	7.4	8.4	8.5
H_8	7.5	7.5	7.7	7.0	7.6	8.1
N_1	−134	−134	−135	−143 (−118)	−128	−132
N_3	−142	−142	−146	−152 (−127)	−136	−141
N_6	−319	−319	−327	−285 (−332)	−310	−322
N_7	−129	−129	−132	−154 (−129)	−123	−128
N_9	−235	−235	−240	−217 (−240)	−226	−234
C_t	177	177	175	7	181	184
H_t	31.3	31.3	31.3	30.6	31.1	30.9
N_n	−159	−159	−166	−299	−152	−139
C_b			37	−99		
N_{py}			−119	−227		
N_{pr}			77	−79		
N_a			171	−8		

[a]BLYP/cc-pVQZ.
[b]BLYP/aug-cc-pV5Z.
[c]BLYP/200 Ry.
[d]PBE/cc-pVQZ.
[e]PBE/100 Ry.

mal variation of about 9 ppm between the ISO and W3 calculations. Larger variations between the ISO and W3 calculations are observed for the hydrogen and nitrogen atoms with 0.6 and 26 ppm, respectively. The last column of the table contains the W5 calculations. The difference between the W3 and W5 is very small with less than 1 ppm for the chemical shift of the carbons, 0.2 ppm for the hydrogens, and 3 ppm for the nitrogens.

While the maximal variation in the chemical shifts with respect to the size of the QM part is small with about 2 ppm for carbon, 0.1 ppm for hydrogen, and 3 ppm for the nitrogen without any N–H bond (N_1, N_3, and N_7), it can be more pronounced with up to 14 ppm for the other nitrogens (N_6 and N_9). This finding reflects the formation of hydrogen bonds between the NH and NH_2 groups with the solvent that are not properly described in the W0 calculation.

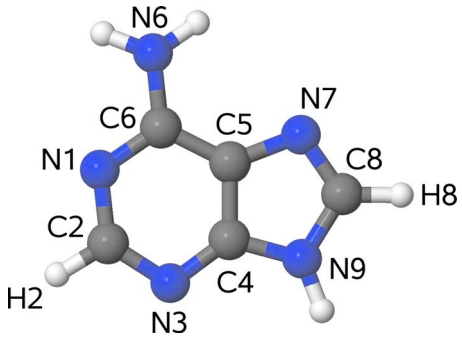

FIG. 3. Labeling scheme for the adenine.

1. g tensor of the E_1' center in α-quartz

To further validate the method for the calculation of the *g* tensor and to apply it in a PBC simulation, we calculated the *g* tensor of the positively charged oxygen vacancy E_1' center in α-quartz. Being one of the most abundant point defects in silica and due to its importance in the degradation of the performance of the gate oxide in transistors, the E_1' center has been the subject of a large number of calculations (an excellent overview can be found in Ref. 56). To our knowledge, the *g* tensor of this defect has been calculated only once,[19] using the GIPAW *g*-tensor method. However, the (periodic) simulation cell that was used included only 71

TABLE V. Calculated ^{13}C, ^{1}H, and ^{15}N chemical shifts of adenine at the BLYP/cc-pVQZ level of theory within a QM/MM framework (see text for details). All the values are in ppm.

	ISO	W0	W3	W5
C_2	164	164	166	166
C_4	148	148	148	148
C_5	120	120	120	120
C_6	160	160	159	159
C_8	145	152	154	154
H_2	7.8	7.8	7.8	7.9
H_8	7.7	8.3	8.2	8.4
N_1	−115	−129	−128	−125
N_3	−127	−147	−144	−145
N_6	−330	−330	−318	−317
N_7	−121	−144	−147	−149
N_9	−249	−237	−226	−223

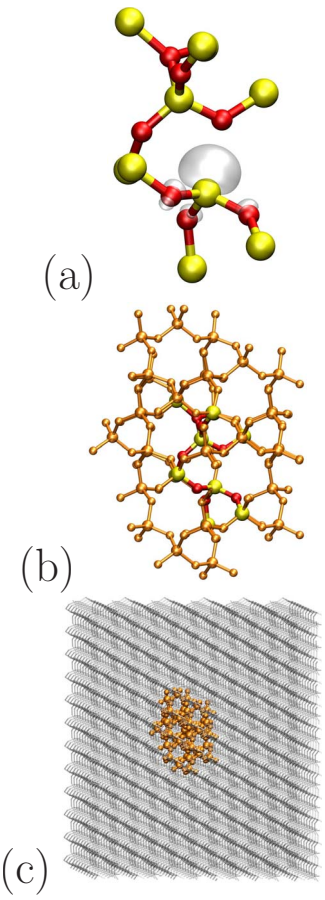

FIG. 4. The hybrid AE/PSP/MM scheme used to describe the E_1' center in α-quartz. The periodically repeated simulation cell has a total of 15 551 atoms, 142 of those are described within the PSP approximation, and another 17 with an AE treatment (i.e., using the full nuclear potential). (a) The AE fragment, together with an isosurface plot of the spin density (ρ^s=0.01 a.u.). (b) The AE fragment embedded in the PSP layer (orange). (c) The QM (AE and PSP) fragment (orange) embedded in the MM layer (gray).

atoms (24 silicon atoms and 47 oxygen atoms), while the real E_1' center in nature has quite a long (up to four to five SiO_2 shells) defect geometry propagation, causing the structure to be somewhat biased by the periodic replica. Moreover, the interaction range of the +1 positive charge of the E_1' center is even much larger than four to five SiO_2 shells, since the quite well ordered structure fails to screen the bare charge.

For the present calculation, we used a QM/MM scheme previously tested and applied on α-quartz.[56–58] The MM α-quartz crystal is made of 15 552 atoms in an orthorhombic cell with lattice constants of 49.94, 57.66, and 63.49 Å, and is described using the van Beest–Kramer–van Santen potential.[59] After removal of an oxygen atom, a portion of 159 QM atoms was chosen in order to surround the oxygen vacancy defect. The geometry was relaxed using the GPW method[37,60] and a PSP approximation for the entire QM subsystem was employed. For the CSGT-GAPW g-tensor calculation on the relaxed structure, 17 QM atoms are described with AE treatment (using the full nuclear potential), while the remaining 142 QM atoms are still described within the PSP approximation. The different subsystems of this approach, which will be referred to as AE/PSP/MM, are shown in Fig. 4. We also performed a calculation using an AE treatment for the entire QM subsystem; this approach will be referred to as AE/MM. A PBE gradient-corrected functional was used (in correspondence with the GIPAW calculation), together with a TZV2P-PSP (Ref. 61) basis set for the PSP atoms and a 6-311G(d,p) basis set for the AE atoms and a 320 Ry cutoff for the auxiliary plane wave grid.

The calculated Δg tensors are presented in Table VI, together with the corresponding experimental[62] and theoretical (using the GIPAW method) data from literature. Comparing the calculated Δg tensors with the available experimental data, all three methods, CSGT-GAPW AE/PSP/MM, CSGT-GAPW AE/MM, and GIPAW, are found to perform very well.

In the GIPAW approach the principal values are slightly overestimated and the quasidegeneracy of the Δg_{yy} and Δg_{zz} principal values is not found. The latter also affects the predictions for the corresponding principal directions. The CSGT-GAPW AE/PSP/MM approach gives a slightly better agreement with experiment compared to the CSGT-GAPW AE/MM, but the differences are minor. An important advantage of the CSGT-GAPW AE/PSP scheme is the lower computational cost compared to a full AE treatment of the QM subsystem. We further refrain from making a strong or definite judgment on the accuracies that can be obtained with the GIPAW and GAPW method, as each method has of course its merits and indeed several influences have not been taken into account in this benchmark, such as level-of-theory effects, dynamical effects and additional structural influences.

IV. SUMMARY

We introduced a method for the AE calculation of the NMR chemical shifts and EPR g tensor with PBC using the GAPW method. Thanks to the AE-GAPW scheme, we can avoid the use of the pseudopotential approximation, which is one of the main sources of inaccuracies for the calculations performed with the original Sebastiani and Parrinello imple-

TABLE VI. Principal values and principal directions of the calculated Δg tensors for the E_1' center in α-quartz and corresponding experimental (Ref. 62) and theoretical (using the GIPAW method) data from literature. Principal values are expressed in ppm and principal directions in degrees.

	Expt.			GAPW AE/PSP/MM			GAPW AE/MM			GIPAW		
	Δg_{ii}	θ	φ	Δg_{ii}	θ	φ	Δg_{ii}	θ	φ	Δg_{ii}	θ	φ
Δg_{xx}	−530	114.5°	227.7°	−561	108.3°	229.6°	−593	108.3°	230.1°	−651	110.0°	223.5°
Δg_{yy}	−1790	134.5°	344.4°	−1830	157.6°	372.8°	−1870	149.0°	353.6°	−2255	142.3°	341.6°
Δg_{zz}	−2020	125.4°	118.7°	−1898	102.5°	135.4°	−1901	114.1°	131.5°	−2481	120.4°	121.1°

mentation, in particular for elements heavier than hydrogen. The method has been validated over a set of small isolated molecules by comparing the deviation of the chemical shifts and g tensor with other theoretical methods. Then, two exemplary applications of the method have been presented, i) a QM/MM calculation of the chemical shifts of an adenine molecule hydrated in a box of 827 water molecules with up to 66 atoms in the QM part and ii) the calculation of the g tensor for the E_1' center in α-quartz using a 15 551-atom simulation cell and a three-layered AE/PSP/MM approach with 159 atoms in the QM (AE/PSP) part. These examples are illustrative of the application field in which we hope the proposed method to be of great value.

ACKNOWLEDGMENTS

This work was supported by the Swiss National Science Foundation (Grant No. 200020-119829), the Fund for Scientific Research-Flanders, and the Research Board of Ghent University.

APPENDIX: EVALUATION OF THE EFFECTIVE POTENTIAL

The effective potential, V_{eff}^{τ}, is split up in a soft global component $\tilde{V}_{\text{eff}}^{\tau,\text{PSP}}$ or $\tilde{V}_{\text{eff}}^{\tau,\text{AE}}$ and local atom-centered components $V_{\text{eff}A}^{\tau,\text{PSP}}$ or $V_{\text{eff}A}^{\tau,\text{AE}}$ depending whether a pseudopotential or a nuclear Coulomb potential is considered, as

$$\tilde{V}_{\text{eff}}^{\tau,\text{PSP}}(\mathbf{r}) = \sum_{A\in\text{PSP}} V_{\text{loc,sr},A}^{\text{PSP}}\theta\left(\alpha_c - \frac{1}{2r_{\text{loc},A}^2}\right) + v_{\text{H}}[\tilde{\rho}(\mathbf{r}) + \rho^0(\mathbf{r})] + v_{X_\alpha}^{\tau}[\tilde{\rho}(\mathbf{r})],$$

$$\tilde{V}_{\text{eff}}^{\tau,\text{AE}}(\mathbf{r}) = v_{\text{H}}[\tilde{\rho}(\mathbf{r}) + \rho^0(\mathbf{r})] + v_{X_\alpha}^{\tau}[\tilde{\rho}(\mathbf{r})],$$

$$V_{\text{eff}A}^{\tau,\text{PSP}}(\mathbf{r}) = V_{\text{loc,sr},A}^{\text{PSP}}(\mathbf{r})\theta'\left(\alpha_c - \frac{1}{2r_{\text{loc},A}^2}\right) + v_{\text{H}}[\rho_A(\mathbf{r}) + \rho_A^c(\mathbf{r})] - v_{\text{H}}[\tilde{\rho}_A(\mathbf{r}) + \rho_A^0(\mathbf{r})] + v_{X_\alpha}^{\tau}[\rho_A(\mathbf{r})] - v_{X_\alpha}^{\tau}[\tilde{\rho}_A(\mathbf{r})],$$

$$V_{\text{eff}A}^{\tau,\text{AE}}(\mathbf{r}) = \frac{Q_A}{r}\text{erfc}\left(\frac{r}{\sqrt{2}r_{\text{loc},A}}\right) + v_{\text{H}}[\rho_A(\mathbf{r}) + \rho_A^c(\mathbf{r})] - v_{\text{H}}[\tilde{\rho}_A(\mathbf{r}) + \rho_A^0(\mathbf{r})] + v_{X_\alpha}^{\tau}[\rho_A(\mathbf{r})] - v_{X_\alpha}^{\tau}[\tilde{\rho}_A(\mathbf{r})],$$

where the appropriate screening densities ρ^0, ρ_A^0, and ρ_A^c are defined in Ref. 25, $\theta(x)$ is the Heaviside function, and $\theta'(x) = -(\theta(x) - 1)$. The factor $\theta'(x)$ causes $V_{\text{loc,sr},A}^{\text{PSP}}$, the short-range part of the pseudopotential for the Ath nucleus, to be included either in the global or in the appropriate local component, depending on whether the decay of the exponential factor in $V_{\text{loc,sr},A}^{\text{PSP}}$ is slower or faster than $e^{-\alpha_c r^2}$. The parameter α_c is an adjustable cutoff. We thus neglect the nonlocal component of the pseudopotentials, which only operates in the close surroundings of the corresponding atomic nucleus. The long-range behavior of the pseudopotentials remains preserved, therefore they still provide the correct contributions in the region of the simulation cell which requires an AE treatment. The soft $\tilde{V}_{\text{eff}}^{\tau}$ is constructed in reciprocal space and subsequently its spatial derivatives are computed. $V_{\text{eff}A}^{\tau,\text{PSP}}$ and $V_{\text{eff}A}^{\tau,\text{AE}}$ quickly go to zero for large distance and this effect is even amplified for their spatial derivatives. We therefore assume that $\nabla V_{\text{eff}A}^{\tau,\text{PSP}}$ and $\nabla V_{\text{eff}A}^{\tau,\text{AE}}$ are only significant within U_A.

[1] P. Hohenberg and W. Kohn, Phys. Rev. **136**, B864 (1964).
[2] W. Kohn and L. J. Sham, Phys. Rev. **140**, A1133 (1965).
[3] M. Kaupp, M. Bühl, and V. G. Malkin, *Calculations of NMR and EPR Parameters: Theory and Applications* (Wiley-VCH, Weinheim, 2004).
[4] C. Ochsenfeld, J. Kussmann, and F. Koziol, Angew. Chem. Int. Ed. **43**, 4485 (2004).
[5] J. Kussmann and C. Ochsenfeld, J. Chem. Phys. **127**, 054103 (2007).
[6] G. Lippert, J. Hutter, and M. Parrinello, Theor. Chem. Acc. **103**, 124 (1999).
[7] M. Krack and M. Parrinello, Phys. Chem. Chem. Phys. **2**, 2105 (2000).
[8] M. Iannuzzi, T. Chassaing, T. Wallman, and J. Hutter, Chimia **59**, 499 (2005).
[9] S. Baroni, P. Giannozzi, and A. Testa, Phys. Rev. Lett. **58**, 1861 (1987).
[10] X. Gonze, Phys. Rev. A **52**, 1086 (1995).
[11] X. Gonze, Phys. Rev. A **52**, 1096 (1995).
[12] A. Putrino, D. Sebastiani, and M. Parrinello, J. Chem. Phys. **113**, 7102 (2000).
[13] D. Sebastiani and M. Parrinello, J. Phys. Chem. A **105**, 1951 (2001).
[14] S. Piana, D. Sebastiani, P. Carloni, and M. Parrinello, J. Am. Chem. Soc. **123**, 8730 (2001).
[15] D. Sebastiani and M. Parrinello, J. Phys. Chem. **108**, 2807 (2004).
[16] R. Declerck, V. Van Speybroeck, and M. Waroquier, Phys. Rev. B **73**, 115113 (2006).
[17] F. Mauri, B. G. Pfrommer, and S. G. Louie, Phys. Rev. Lett. **77**, 5300 (1996).
[18] C. J. Pickard and F. Mauri, Phys. Rev. B **63**, 245101 (2001).
[19] C. Pickard and F. Mauri, Phys. Rev. Lett. **88**, 086403 (2002).
[20] F. London, J. Phys. Radium **8**, 397 (1937).
[21] R. Ditchfield, Mol. Phys. **27**, 789 (1974).
[22] T. A. Keith and R. F. W. Bader, Chem. Phys. Lett. **194**, 1 (1992).
[23] T. A. Keith and R. F. W. Bader, Chem. Phys. Lett. **210**, 223 (1993).
[24] R. Declerck, E. Pauwels, V. V. Speybroeck, and M. Waroquier, Phys. Rev. B **74**, 245103 (2006).
[25] P. E. Blöchl, Phys. Rev. B **50**, 17953 (1994).
[26] R. Resta, Phys. Rev. Lett. **80**, 1800 (1998).
[27] G. H. Wannier, Phys. Rev. **52**, 191 (1937).
[28] N. Marzari and D. Vanderbilt, Phys. Rev. B **56**, 12847 (1997).
[29] G. Berghold, C. Mundy, A. Romero, J. Hutter, and M. Parrinello, Phys. Rev. B **61**, 10040 (2000).
[30] C. Brouder, G. Panati, M. Calandra, C. Mourougane, and N. Marzari, Phys. Rev. Lett. **98**, 046402 (2007).
[31] J. R. Cheeseman, G. W. Trucks, T. A. Keith, and M. J. Frisch, J. Chem. Phys. **104**, 5497 (1996).
[32] V. I. Lebedev, Zh. Vychisl. Mat. Mat. Fiz. **15**, 48 (1975).
[33] V. I. Lebedev, Zh. Vychisl. Mat. Mat. Fiz. **16**, 293 (1976).
[34] G. Schreckenbach and T. Ziegler, J. Phys. Chem. A **101**, 3388 (1997).
[35] J. C. Slater, Phys. Rev. **81**, 385 (1951).
[36] The CP2K developers group, 2008, http:/cp2k.berlios.de/.
[37] J. VandeVondele, M. Krack, F. Mohamed, M. Parrinello, T. Chassaing, and J. Hutter, Comput. Phys. Commun. **167**, 103 (2005).
[38] M. J. Frisch, G. W. Trucks, H. B. Schlegel *et al.*, GAUSSIAN 03, Revision C.01, Gaussian, Inc., Wallingford, CT, 2004.
[39] ADF2007, 01, SCM, Theoretical Chemistry, Vrije Universiteit, Amsterdam, The Netherlands, 2007, http://www.scm.com/.
[40] A. D. Becke, Phys. Rev. A **38**, 3098 (1988).
[41] C. Lee, W. Yang, and R. G. Parr, Phys. Rev. B **37**, 785 (1988).
[42] V. Weber, J. VandeVondele, J. Hutter, and A. M. N. Niklasson, J. Chem. Phys. **128**, 084113 (2008).
[43] K. Schuchardt, B. Didier, T. Elsethagen, L. Sun, V. Gurumoorthi, J. Chase, J. Li, and T. Windus, J. Chem. Inf. Model. **47**, 1045 (2007).
[44] P. Hariharan and J. Pople, Theor. Chim. Acta **28**, 213 (1973).
[45] M. Francl, W. Petro, W. Hehre, J. Binkley, M. Gordon, D. DeFrees, and J. Pople, J. Chem. Phys. **77**, 3654 (1982).
[46] T. H. Dunning, J. Chem. Phys. **90**, 1007 (1989).
[47] D. E. Woon and T. H. Dunning, J. Chem. Phys. **100**, 2975 (1994).
[48] R. A. Kendall, T. H. Dunning, and R. J. Harrison, J. Chem. Phys. **96**, 6796 (1992).

[49] D. E. Woon and T. H. Dunning, J. Chem. Phys. **98**, 1358 (1993).
[50] QUANTUM-ESPRESSO is a community project for high-quality quantum-simulation software, based on density-functional theory, and coordinated by P. Giannozzi, 2008, http://www.quantum-espresso.org/.
[51] N. Troullier and J. L. Martins, Phys. Rev. B **43**, 1993 (1991).
[52] J. P. Perdew, K. Burke, and M. Ernzerhof, Phys. Rev. Lett. **77**, 3865 (1996).
[53] CPMD, program package, copyright IBM Corp. 1990–2004, copyright MPI für Festkörperforschung Stuttgart, 2001, http://www.cpmd.org/.
[54] C. Hartwigsen, S. Goedecker, and J. Hutter, Phys. Rev. B **58**, 3641 (1998).
[55] S. Komin, C. Gossens, I. Tavernelli, U. Rothlisberger, and D. Sebastiani, J. Phys. Chem. B **111**, 5225 (2007).
[56] T. Laino, D. Donadio, and I. W. Kuo, Phys. Rev. B **76**, 195210 (2007).
[57] F. Zipoli, T. Laino, A. Laio, M. Bernasconi, and M. Parrinello, J. Chem. Phys. **124**, 154707 (2006).
[58] T. Laino, A. Mohamed, and M. Parrinello, J. Chem. Theory Comput. **2**, 1370 (2006).
[59] W. H. van Beest, G. J. Kramer, and R. A. van Santen, Phys. Rev. Lett. **64**, 1955 (1990).
[60] G. Lippert, J. Hutter, and M. Parrinello, Mol. Phys. **92**, 477 (1997).
[61] G. Lippert, J. Hutter, P. Ballone, and M. Parrinello, J. Phys. Chem. **100**, 6231 (1996).
[62] M. G. Jani, R. B. Bossoli, and L. E. Halliburton, Phys. Rev. B **27**, 2285 (1983).